[Research Paper] 대한금속 · 재료학회지 (*Korean J. Met. Mater.*), Vol. 60, No. 7 (2022) pp.517-522
DOI: 10.3365/KJMM.2022.60.7.517

Enhanced Photoelectrochemical Water-Splitting through Application of Layer by Layer (LBL) and Hydrothermal (HT) Methods in TiO_2 and α-Fe_2O_3 Hierarchical Structures

Aryan Azad[1,2] and Sun Jae Kim[1,*]

[1]*Faculty of Nanotechnology and Advanced Materials Engineering, Sejong University, Seoul 143-747, Republic of Korea.*
[2]*Future Industries Institute, University of South Australia, Mawson Lakes 5095, Australia*

Abstract: Improving solar energy conversion efficiency and reducing energy loss have become critical issues in recent decades. Photoelectrochemical (PEC) water splitting provides an ideal method for solar energy harvesting and is a key factor in decreasing the use of fossil fuels. Thus, it is extremely important to identify cost-effective, highly active, and robust semiconducting photoelectrodes that can reduce the overpotential reaction and increase electrocatalytic efficiency. However, for overall water splitting, it is challenging to identify suitable photocatalysts with efficient band structures and suitable charge separation for electron-hole pairs. Water splitting is conventionally performed using independent layer-by-layer (LBL) or hydrothermal (HT) techniques. However, this research aims to produce a photoanode by applying both HT and LBL methods in sequence to reduce energy loss during the electron transfer process between the two photosystems. In this study, a TiO_2 layer was deposited onto fluorine tin oxide (FTO) glass using the LBL method (TiO_2/FTO). Subsequently, hematite (α-Fe_2O_3) thin films that were synthesized using the HT method were deposited onto TiO_2/FTO glasses (Fe_2O_3/TiO_2/FTO). The as-prepared and newly-designed photoanode Fe_2O_3/TiO_2/FTO demonstrates a significantly high photocatalytic activity of 7.68 mA/cm^2. Thus, by combining the HT and LBL methods, excellent hydrogen production performance in regard to photocatalytic water splitting was achieved. Furthermore, this hierarchical structure provides good chemical stability and is an excellent candidate for large-scale applications.

(Received 4 January, 2022; Accepted 30 March, 2022)

Keywords: photoelectrochemical water-splitting, semiconductors, hematite (α-Fe_2O_3), Ti doping, hydrothermal method, doping method

1. INTRODUCTION

The reduction in fossil fuel resources has shifted the conventional energy system in the direction of renewable energy sources such as water, wind, solar, and hydrogen resources. Solar energy provides a promising option for hydrogen production from renewable energy resources [1]. For solar hydrogen generation, photoelectrochemical (PEC) water-splitting has received intense attention during the past decade due to its versatile properties [1]. Hematite (α-Fe_2O_3) is an *n*-type semiconductor candidate for solar water splitting that is earth-abundant and stable and possesses an appropriate band-gap of 2.2 eV that ranges in the visible region [2-4]. It was stable against photocorrosion in alkaline solutions. However, the performance of hematite for solar water splitting is limited by factors such as poor conductivity, oxygen evolution reactions (OER), a short hole diffusion length between 2 and 4 nm, a short lifetime of the excited-state carrier between 10 and 12 s, and improper band positions [2-9]. TiO_2 is another important transition metal oxide that displays a favorable band edge position, strong optical absorption, and an inexpensive cost [1,10-12]. It can be used as a photoanode for water-splitting, batteries, dye removal, supercapacitors, and other applications [13]. A number of factors such as the phase structure, surface area, crystallite size, and number of surface hydroxyl groups directly influence the photocatalytic performance of TiO_2 [14,15]. In contrast, one of the key impediments to improving photocatalytic efficiency is the restriction of the recombination of electrons and holes [14,16]. Hence, developing approaches that can promote charge separation in TiO_2 is highly

- Aryan Azad: 박사 후 연구원, 김선재: 교수
**Corresponding Author:* Sun Jae Kim
[Tel: +82-2-3408-3780, E-mail: sjkim1@sejong.ac.kr]

desired [14-17]. Various methods such as synthesizing branched structures [18,19], doping with metal or non-metal elements [20-24], post-growth hydrogen annealing, sensitizing with other small bandgap semiconductor materials, and controlling the crystallite size and structure have been implemented to improve the photocatalytic properties of TiO_2 nanomaterials [25]. The different crystal structures of TiO_2 (rutile and anatase) are the most significant factors that influence photocatalytic performance [10,17]. For improving the performance of hematite, elemental doping has been also studied using [26,27] Si and Sn, and they can be prepared by different methods to increase the photocurrent density at low bias by reducing electron-hole recombination and enhancing donor density beyond a few picoseconds [26-31]. This study aims to design a photoanode material while also discussing the key parameters that affect the photocatalytic behavior of Fe_2O_3/TiO_2/FTO. Surprisingly, the design of a new photoanode demonstrates excellent photocatalytic activity by decreasing the bandgap energy and reducing electron-hole recombination.

2. EXPERIMENTS

2.1 α-Fe_2O_3/FTO hydrothermal (F HT/FTO)

For the hydrothermal coating of α-Fe_2O_3/FTO, fluorine-doped SnO_2 glass (FTO, 14 Ω sq^{-1}, Asahi Glass Co., Japan) was used as the substrate. The FTO glass was cleaned using acetone, ethanol, and deionized water. A mixture of 0.85 g of $NaNO_3$ and 0.4 g of $FeCl_3.6H_2O$ at pH 1.5 (adjusted with HCl) was then prepared. A piece of clean FTO glass (3 cm × 3 cm × 2 mm) was placed within the vial and heated at 100 °C for 6 h in an autoclave. A thin layer of yellow FeOOH was formed on the FTO substrate. When the samples were cooled to room temperature, the coated FeOOH on the substrates was cleaned with deionized water and dried at 80 °C. The phase transition to α-Fe_2O_3 from β-FeOOH was achieved by annealing for 2 h at 550 °C. The samples were annealed again at 750 °C for 10 min. This additional heat treatment did not affect morphology formation; however, it prompted the formation of the target composition (from the oxyhydroxide phase to the designed hematite phase).

2.2 Ti- Fe_2O_3/FTO hydrothermal (T-F HT/FTO)

To achieve Ti-doped Fe_2O_3/FTO, a piece of cleaned FTO glass (3 cm × 3 cm × 2 mm) was placed into a vial containing 0.85 g of $NaNO_3$, 0.4 g of $FeCl_3.6H_2O$ at pH 1.5 (adjusted by HCl), and 0.5 ml titanium carbonitride (TiCN, Sigma-Aldrich). An aqueous solution was added as a precursor (10 mg/ml) to the solution. The vial was then transferred to an autoclave and heated for 6 h at 100 °C. Consequently, TiCN was created as a thin black layer on the FTO glass. The extra black powder was removed from the synthesized samples using deionized water prior to sintering in air. The samples were then annealed at 550 °C for 2 h. and then heat-treated at 750 °C for an additional 10 min as described above.

2.3 TiO_2/FTO Layer by Layer (T LBL/FTO)

In the layer-by-layer self-assembly method (LBL), the cleaning process for FTO glass was different. In this method, the FTO surface must be fresh and ready to accept ions with different charges. Therefore, piranha solution (7:3 = 70 % conc. H_2SO_4:30 % H_2O_2) was used to treat the surface of the FTO glass. Each piece of FTO glass was etched for 20 min by dipping into 0.2 M polyethyleneimine (PEI, Aldrich Co.) at room temperature to create a positive charge on the FTO glass. Subsequently, ions with negative charges were fabricated by immersing the FTO glass for 20 min in 10 gL^{-1} of aqueous hydrogen titanate (H-TiNT) (powder obtained by a hydrothermal technique [32]) dispersed with 0.2 M tetra butyl ammonium hydroxide (TBAOH, Aldrich Co.). The same method was used to obtain a layer of positively charged ions. The FTO-treated films were immersed in 0.2 M poly diallyl dimethyl ammonium chloride (PDDA, Aldrich Co.). To clean the FTO glasses of all surfactants such as PEI, TBAOH, and PDDA and to obtain H-TiNT/FTO, UV-Vis light irradiation (Hg-Xe 200 W lamp, Super-cure, SAN-EI Electric) was used. Finally, the TiO_2/FTO (T LBL/FTO) thin film samples were heated inside a box furnace at a heating rate of 500 °C h^{-1} and then annealed for 10 min.

2.4 Fe_2O_3/TiO_2/FTO photoanodes prepared by layer-by-layer (LBL) and hydrothermal (HT) methods (F HT/T LBL/FTO)

To prepare the Fe_2O_3/TiO_2/FTO photoanode, the TiO_2/FTO (LBL) sample from section 2.3 was placed into a vial (stainless steel shell and Teflon liner) containing a 0.85 g of $NaNO_3$ and 0.4 g of $FeCl_3.6H_2O$ at pH 1.5 (adjusted with

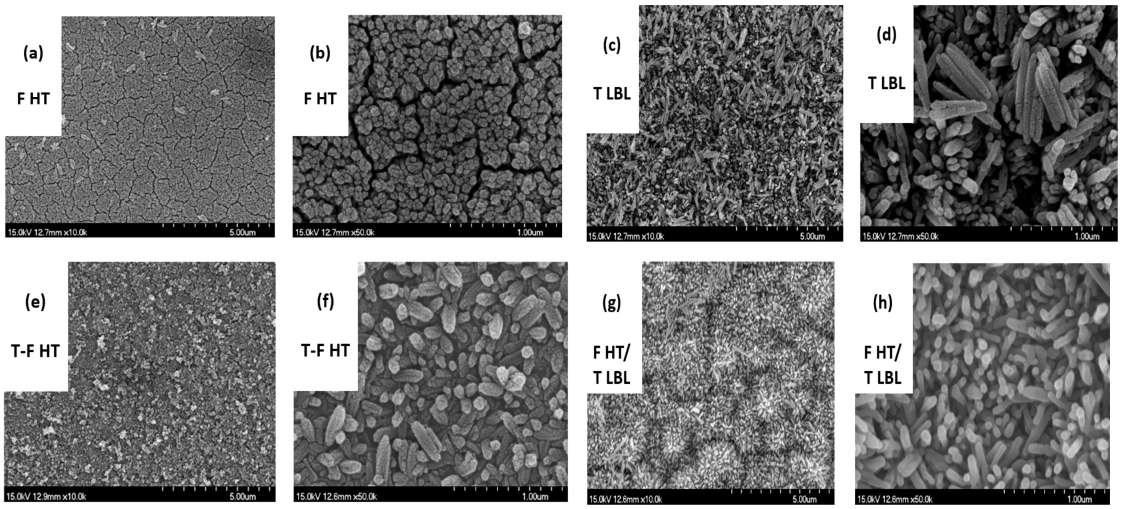

Fig. 1. SEM micrographs at 10,000× and 50,000× magnification of 4 different photoanodes: (a, b) F HT/FTO sintered at 550 °C for 2 h with additional heat treatment at 750 °C for 10 min, (c, d) T LBL/FTO sintered at 500 °C for 10 min, (e, f) T-F HT/FTO sintered at 550 °C for 2 h. with additional heat treatment at 750 °C for 10 min, and (g, h) F HT/ T LBL/ FTO sintered at 550 °C for 2 h with additional heat treatment at 750 °C for 10 min.

HCl) solution. It was then placed in an autoclave and heated to 100 °C for 6 h. The sample was washed with deionized water after cooling to room temperature and then dried at 80 °C. To obtain the α-Fe_2O_3 phase, β-FeOOH samples were annealed at 550 °C for 2 h. The samples were annealed at 750 °C for an additional 10 min to facilitate the formation of the target phase.

3. RESULTS AND DISCUSSION

Manipulating particle size is a general strategy to improve the quality of a photocatalyst. Reducing the particle size of a photocatalyst enhances the density of the catalytic site surface and the photocatalytic activity due to the shortened diffusion length of photogenerated electron-hole pairs [33]. The surface morphology and particle sizes of F HT/FTO, T LBL/FTO, T-F HT/FTO, and F HT/ T LBL/FTO sintered at different temperatures (500, 550, and 750 °C) are presented in the FESEM images in Figure 1 that illustrate different nanostructures. Figures 1 (a) and (b) present the uniform distribution of the nanorods of F-HT nanostructures on the FTO substrates. The growth of TiO_2 by the LBL method on the FTO glass substrates exhibited short nanorod-like structures as indicated in Figures 1 (c) and (d). The T-F HT/ FTO sample presented in Figures 1 (e) and (f) exhibits short urchin-like structures. Figure 1 (g, h) presents sample F HT/

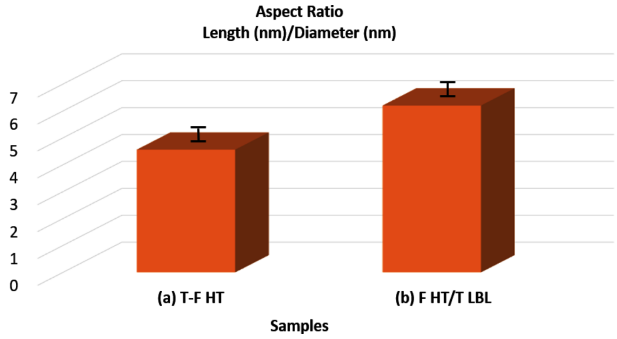

Fig. 2. Aspect ratio of samples (a) T-F HT sintered at 550 °C for 2 h with additional heat treatment at 750 °C for 10 min and (b) F HT/ T LBL sintered at 550 °C for 2 h.

T LBL/ FTO that was synthesized by both LBL and HT methods in sequence and exhibits a short urchin-like structure. Therefore, samples exhibiting urchin-like nanostructures possess smaller feature sizes that may increase the aspect ratio of the effective interface of hematite and could be suitable for photoelectrochemical splitting. Furthermore, the smaller feature size causes the photogeneration of holes that are closer to the semiconductor liquid junction (SCLJ) [34]. Figure 2 indicates the aspect ratios of two samples with urchin-like structures.

X-ray diffraction (XRD, Rint-2000, Rigaku) was performed with Cu Kα radiation (λ=1.54056 Å) at 40 kV and 100 mA at a scanning speed of 2 ° min^{-1}. Figure 3 presents the XRD data for samples (a) F HT/ T LBL, (b) T-F HT, and (c) F HT

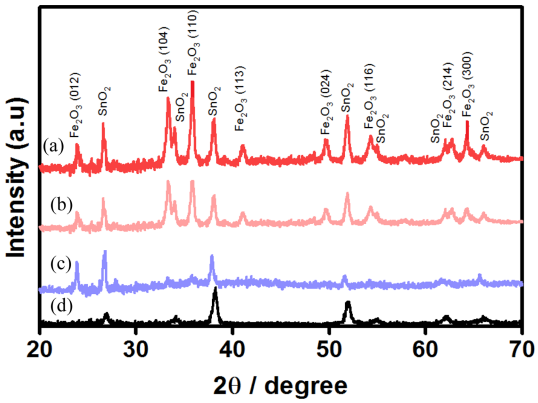

Fig. 3. XRD spectra for (a) F HT/ T LBL, (b) T-F HT, (c) F HT, and (d) FTO glass.

and for (d) bare FTO glass. T-F HT sample (b) exhibits enhanced crystallinity of hematite compared to that of sample (c) as observed from the increased intensity of the (110) and (104) peaks (the intensity of the [110] peak in T-F HT is stronger than is that of F HT). A general comparison of the intensity of the (110) XRD peak revealed that the sample F HT/ T LBL that was sintered at 550 °C for 2 h. with an additional heat treatment for 10 min at 750 °C yielded the best crystallinity. As described, the use of both the HT and LBL methods reduces the feature size, and this ultimately leads to improved crystallinity.

The measured photoelectrochemical performance of a 1 M aqueous solution of NaOH electrolyte is presented in Figure 4. The counter and reference electrodes were platinum (Pt) wire and saturated calomel electrode (SCE) Hg/Hg_2Cl_2, respectively, as illustrated in Figure 4 (1). Different substrate-based photoelectrochemical cells that were sintered at 500, 550, and 750 °C were used as working electrodes in the dark and under light illumination (100 mW cm^{-2} UV-Vis). The range of linear sweep voltammetry was between 0.0~+1.8 (V versus RHE). The photocurrent at 1.23 V_{RHE} was increased for samples (c), (b), and (a) as illustrated in Figure 4 (3), and the highest value of 2.04 mA cm^{-2} was observed for sample (a). Sample (c) T LBL at 1.23 V vs RHE exhibited a low photocurrent density of 1.02 mA/cm^2 as presented in Figure 4 (3). The photocurrent density of F-HT (sample [b]) at 1.23 V vs. RHE was observed at 1.84 mA/cm^2.

The addition of TiCN as a precursor to the HT method resulted in the formation of new hematite nanostructures possessing an urchin-like morphology. In this structure, the

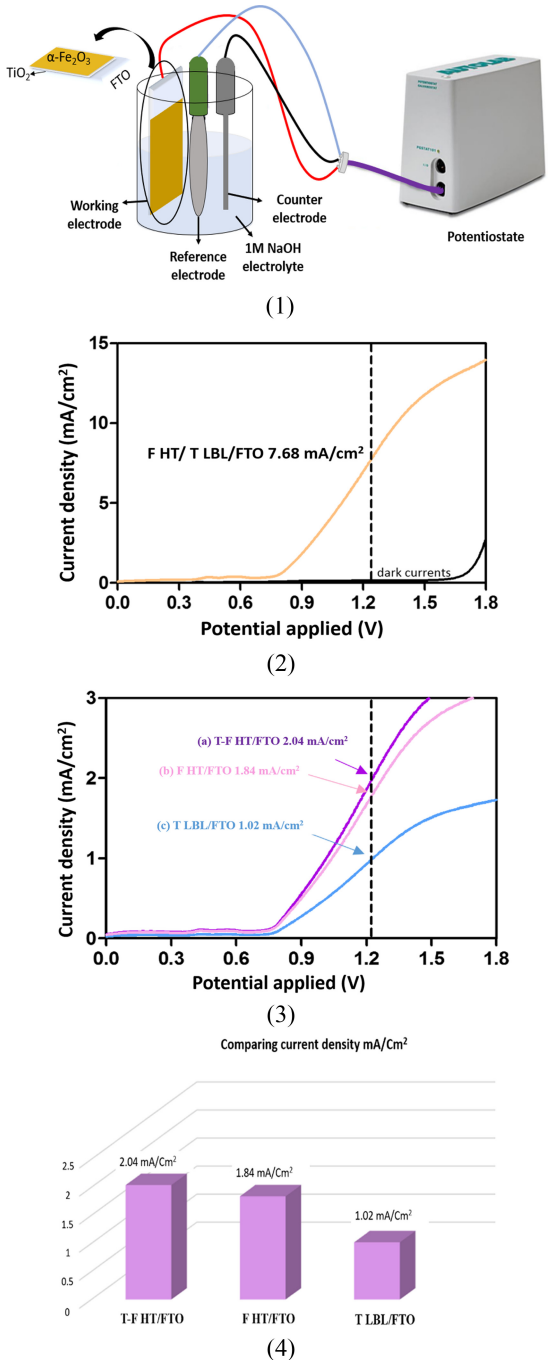

Fig. 4. (1) Schematic of photoelectrochemical performance of sample F HT/ T LBL as a working electrode that was sintered at 550 °C for 2 h with additional heat treatment for 10 min at 750 °C in a 1 M aqueous solution of NaOH electrolyte. (2) *I-V* characteristics of F HT/ T LBL sintered at 550 °C for 2 h with additional heat treatment for 10 min at 750 °C, (3) (a) T-F HT sintered at 550 °C 2 h with additional heat treatment for 10 min at 750 °C, (b) F HT sintered at 550 °C for 2 h with additional heat treatment for 10 min at 750 °C, and (c) T LBL sintered at 500 °C for 10 min. For all the measurements, the simulated solar illumination was 100 mW cm^2, and 1.0 M NaOH was used as an aqueous electrolyte. (4) Comparison of photocurrent densities for samples (a)-(c).

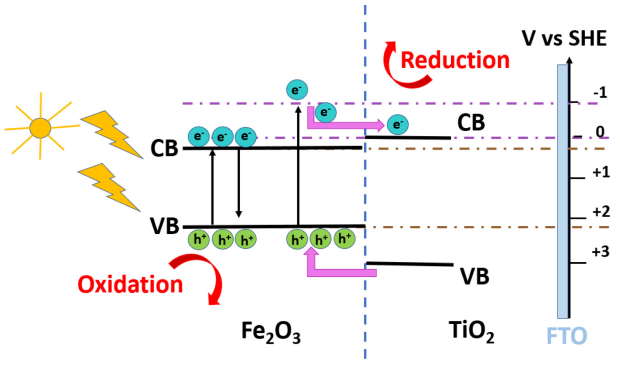

Fig. 5. Schematic of the mechanism for enhancing the photocatalytic properties of F HT/ T LBL/ FTO.

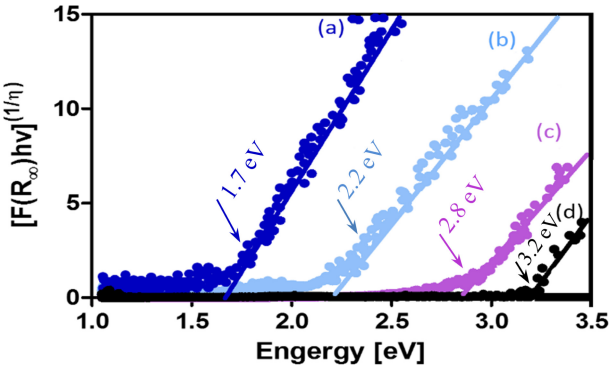

Fig. 6. Optical absorbances of the (a) F HT/ T LBL sintered at 550 °C for 2 h with additional heat treatment for 10 min at 750 °C, (b) T-F HT sintered at 550 °C 2 h with additional heat treatment for 10 min at 750 °C, (c) F HT sintered at 550 °C for 2 h with additional heat treatment for 10 min at 750 °C, and (d) T LBL sintered at 500 °C for 10 min.

electron-hole recombination is reduced and a high photocurrent density at 1.23 V vs. RHE is obtained. The achieved current densities for samples (a)-(c) are compared in Figure 4 (4). The photocurrent density of sample F HT/ T LBL at 1.23 V vs. RHE was remarkably increased as shown in Figure 4 (2) due to the use of a TiO_2 underlayer. TiO_2 acts as a barrier layer and prevents electrons from recombining in F HT/ T LBL photoanodes [35]. Thus, the TiO_2 interlayer plays a significant role in the efficient collection and conversion of photon energy [36].

A schematic of the process for charge transfer and separation in sample F HT/ T LBL /FTO is presented in Figure 5. The photogenerated electrons of α-Fe_2O_3 under visible irradiation can be excited from the valence band (VB) to different energy levels of the conduction band (CB) (including the high-energy and low-energy regions). At a low energy level, the photogenerated electrons quickly relax to the VB bottom of α-Fe_2O_3 to recombine with the holes. However, high-energy electrons are thermodynamically transferred to the CB of TiO_2, thus leading to the promoted separation of visible-excited charges [35-38].

The optical band gap energy presented in Figure 6 reveals the effect of the LBL coating and doping layer arrangement on all four samples. Using both the HT and LBL methods and according to the highest obtained photocurrent density in Figure 4, the bandgap energy is decreased in sample F HT/ T LBL / FTO. Typically, electrons that gain energy that is equal to or greater than the bandgap energy in the valence state are excited to the conduction band. In this study, TiO_2 nanocrystals were the center for recombining electrons and holes. By decreasing the bandgap energy and increasing the photocurrent density, the smaller urchin-like structure of the F HT/ T LBL / FTO sample acted as a photoanode and enhanced PEC water splitting.

4. CONCLUSION

This research study presents an enhanced water-splitting efficiency technique using a novel photoanode designed by utilizing LBL and HT methods. The morphology, particle size, and surface area all play important roles in the improvement of water-splitting performance, and thus, due to these factors and the effect of TiO_2 as a compact layer between FTO and the α-Fe_2O_3 photoanode, the properties and water-splitting process are enhanced. A newly designed Fe_2O_3/TiO_2/FTO (F HT/ T LBL /FTO) photoanode (sintered at 550 °C for 2 h. with an additional heat treatment for 10 min at 750 °C) demonstrated a current density of 7.68 mA/ cm^2. By applying both LBL and HT methods simultaneously, an innovative method is proposed that leads to the formation of urchin-like structures possessing smaller feature particle sizes. Eventually, decreasing the bandgap energy reduces the electron-hole recombination, and this leads to a much higher photoelectrochemical water-splitting efficiency.

ACKNOWLEDGMENT

This work was supported by the National Research Foundation

of Korea (NRF) grant funded by the Ministry of Science, ICT, and Future planning [NRF-2018K1A4A3A01064272] and [NRF-2020R1A6A1A03038540].

REFERENCES

1. Arifin K, Yunus R. M, Minggu L. J, and Kassim M. B, *Int. J. Hydrog. Energy.* **46**, 4998 (2021).
2. Kyesmena P. I, Nombonab N, and Dialea M, *J. Alloys Compd.* **863**, 158724 (2021).
3. Feng H, Feng S, Tang N, Zhang S, Zhangd X, and Liud B, *RSC Adv.* **11**, 10300 (2021).
4. Reli M, Ambrožová N, Valášková M, Edelmannová M, Čapek L, Schimpf C, Motylenko M Rafaja D, and Kočí K, *Photocatalytic water splitting over CeO2/Fe2O3/Ver photocatalysts*. **238**, 114156 (2021).
5. Mayer MT, Lin Y, Yuan G, and Wang D, *Acc. Chem. Res.* **46**, 1558 (2013).
6. Lin Y, Yuan G, Sheehan S, Zhou S, and Wang D. *Energy Environ. Sci.* **4**, 4862 (2011).
7. Ling Y, Wang G, Wheeler D. A, Zhang J. Z, Li Y, *Nano Lett.* **11**, 2119 (2011).
8. Le Formal F, Gratzel M, and Sivula K, *Adv. Funct. Mater.* **20**, 1099 (2010).
9. Tilley S. D, Cornuz M, Sivula K, and Gratzel M, *Angew. Chem. Int. Ed.* **49**, 6405 (2010).
10. Fu B, Wu Z, Cao S, Guoa K, and Piao L, *Nanoscale.* **12**, 4895 (2020).
11. Zhang T, Lin P, Wei N, and Wang D, *ACS Appl. Mater. Interfaces.* **12**, 20110 (2020).
12. Liu M, Qiu X, Miyauchi M, and Hashimoto K, *Chem. Mater*. **23**, 5282 (2011).
13. Anil Kumar M. R, Abebe B, Nagaswarupa H. P, Ananda Murthy H. C, Ravikumar C. R, and Kedir Sabir F, *Scientific Reports* **10**, 1249 (2020).
14. Cao S, Chan T. S, Lu Y. R, Shi X, Fu B, Wu Z, Li H, Liu K, Alzuabi S, Cheng P, Liu M, Li T, Chen X, and Piao L, *Nano Energy* **67**, 104287 (2020).
15. Puddu V, Choi H, Dionysiou D. D, and Puma G. L. *Appl. Catal. B: Environ* **94**, 211 (2010).
16. Rivera A, Tanaka K, and Hisanaga T, *Appl. Catal. B: Environ* **3**, 37 (1993).
17. Karakitsou K. E and Verykios X. E, *J. Phys. Chem.* **97**, 1184 (1993).
18. Reddy C. V, Reddy K. R, Shetti N. P, Shim J, Aminabhavi T. M, and Dionysiou D. D, *Int. J. Hydrog. Energy.* **45**, 18331 (2020).
19. Cho I. S, Chen Z, Forman A. J, Kim D. R, Rao P. M, Jaramillo T. F, and Zheng X. *NanoLett.* **11**, 4978 (2011).
20. Hoang S, Guo S, Hahn N. T, Bard A. J, and Mullins C. B, *Nano Lett.* **12**, 26 (2011).
21. Das C, Roy P, Yang M, Jha H, and Schmuki P, *Nanoscale* **3**, 3094 (2011).
22. Zhang R, Fang Y, Chen T, Qu F, Liu Z, Du G, Asiri A. M, Gao T, and Sun X, *ACS Sustainable Chem. Eng.* **5**, 7502 (2017).
23. Deng J, Zhang Q, Feng K, Lan H, Zhong J, Chaker M, and Ma D. *Chem. Sus. Chem.* **11**, 3783 (2018).
24. Liu J, Yang S, Wu W, Tian Q, Cui S, Dai Z, Ren F, Xiao X, and Jiang C. *ACS Sustainable Chem. Eng.* **3**, 2975 (2015).
25. Zhu J, Zheng W, He B, Zhang J, and Anpo M, *J. Mol. Catal. A: Chem.* **216**, 35 (2004).
26. Wang G. M, Li Y. C, Wheeler D. A, George KEN, Horsley K, Heske C, Zhang J. Z, and Li Y, *Nano Lett.* **11**, 3503 (2011).
27. Cesar I, Sivula K, Kay A, Zboril R, and Gratzel M. *J. Phys. Chem. C.* **113**, 772 (2009).
28. Pino A, onzález-Campo A, Giraldo S, Peral J, György E, Logofatu C, DeMello A. J, and Puigmartí-Luisf J, *Carbon* **130**, 48 (2018).
29. Wang F, Shen T, Fu Z, Lu Y, and Chen C, *Nanotechnology* **29**, 1 (2017).
30. Pyeon M, Wang M, Gönüllü Y, Kaouk A, Jäckle S, Christiansen S, Hwang T, Moon K, and Mathur S, *MRS Comunications* **6**, 442 (2016).
31. Acar C, Dincer I, and Naterer G. F, *Int. J. Energy Res.* **40**, 1449 (2016).
32. Oh H. J, Noh K. J, Ku H. K, Jung S. C, Lee W. J, Kang W. S, and Kim S. J, *Prog. Org. Coat.* **74**, 745 (2012).
33. Zhou Z, Yin H, Zhao Y, Zhang J, Li Y, Yuan J, Tang J, and Wang F, *Catalysts* **11**, 396 (2021).
34. Sivula K, Formal F. L, and Grtzel M, *Chem. Sus. Chem.* **4**, 432 (2011).
35. Dekrafft K. E, Wang C, and Lin W. B, *Adv. Mater*. **24**, 2014 (2012).
36. Saito R, Miseki Y, and Sayama K, *Chem. Comm.* **48**, 3833 (2012).
37. Huang R, Liang R, Fan H, Ying S, Wu L, Wang X, and Yan G, *Scientific Reports* **7**, 7858 (2017).
38. Hung W. H, Teng Y. J, Tseng C. M, and Thai Nguyen H. T, *Nanoscale Res Lett* **16**, 76 (2021).